PAPER

In vitro imaging of β-cells using fluorescent cubic bicontinuous liquid crystalline nanoparticles

V. Miceli,[ag] V. Meli,[b] M. Blanchard-Desce,[c] T. Bsaibess,[c] M. Pampalone,[ag]
P. G. Conaldi,[a] C. Caltagirone,[b] M. Obiols-Rabasa,[d] J. Schmidt,[e] Y. Talmon,[e] A. Casu*[f]
and S. Murgia*[b]

To evaluate the potential of monoolein-based cubic bicontinuous liquid crystalline nanoparticles (cubosomes) as diagnostic tools in diabetes and pancreatic β-cell transplantation, fluorescent cubosomes were formulated, entrapping within the lipid bilayer a newly synthesized, potent, hydrophobic dye. Cryo-TEM, SAXS, and DLS were performed to assess the morphological and structural aspects of this formulation. Rat pancreatic β-cells (INS-1E) readily took up the cubosome nanoparticles, as revealed by in vitro internalization tests, and flow-cytometric analyses confirmed the persistence of the fluorescence for up to 24 hours. The cytotoxicity of cubosomes at various concentrations, evaluated with a real-time analysis of proliferation, revealed that the proliferation curves relative to the less concentrated formulation (5 μM in terms of monoolein content) were comparable to the untreated cultures. INS-1E cell cycle and apoptosis supported such results. In conclusion, this formulation, with dye content in the nanomolar range, seems to be useful for β-cell imaging.

1. Introduction

Nanotechnology applied to biomedical science offers unique opportunities to revolutionize the treatment of numerous diseases by exploiting nanomedicines, probably the most relevant outcome belonging to the merging of these two research domains. Nanomedicines are carriers with size in the sub-micrometer range, developed with the aim of improving the biodistribution of systemically administered diagnostic or therapeutic agents, improving treatment efficacy, and reducing undesirable side effects.[1,2] Nanomedicine can combine multiple modalities on a single carrier, allowing for deeper understanding of in vivo processes. Their ability to simultaneously deliver drugs and imaging probes has paved the way for the advent of a new generation of theranostics.[3] So far several nanomedicine formulations, including liposomes and polymeric nanoparticles, have been approved for clinical use by the FDA,[4] and many others are currently under investigation. Among them, lipid-based cubic bicontinuous liquid crystalline nanoparticles, known as cubosomes, represent an emerging platform for the co-delivery of drugs and imaging probes.[5,6] Indeed, similarly to the bulk bicontinuous cubic phases to which they belong,[7] cubosomes possess an inner nanostructure characterized by curved, triply periodic, non-intersecting lipid bilayers, where hydrophobic molecules of biomedical or pharmaceutical interest can be hosted.[8–11] Remarkably, these bilayers are arranged in space to form two disconnected and continuous water channels. Cubosomes are often regarded as the non-lamellar counterpart of liposomes, though, per unit of volume, they offer a higher hydrophobic volume and a larger surface exposed to water.[12] Furthermore, their surface can be decorated with targeting residues to actively direct these nanoparticles towards specific tissues.[13–15]

Several recent papers have explored the potential of cubosomes in cancer treatments. However, other equally severe pathologies, such as diabetes, could take advantage of this kind of nanoparticle. Type 1 diabetes (T1D) is a metabolic disease caused by the autoimmune destruction of the pancreatic β-cells, located in the islets of Langerhans in the pancreas. β-Cells produce and secrete insulin, a peptide hormone implicated in the maintenance of normal blood glucose levels. Chronic elevation of glucose in the blood of T1D patients causes vessel and organ dysfunction, which worsen quality of life, and cause premature death. Despite the increasing incidence of T1D worldwide, the questions of early

[a]Department of Laboratory Medicine and Advanced Biotechnologies, IRCCS-ISMETT (Istituto Mediterraneo per iTrapianti e Terapie ad Alta Specializzazione), via Tricomi 5, 90127 Palermo, Italy

[b]Department of Chemical and Geological Science, University of Cagliari, CNBS, CSGI, s.s. 554 bivio per Sestu, 09042 Monserrato CA, Italy. E-mail: murgias@unica.it; Tel: +39 070 675 4453

[c]University of Bordeaux, Institut des Sciences Moléculaires, (CNRS UMR 5255), 33 405 Talence, France

[d]Division of Physical Chemistry, Department of Chemistry, Naturvetarvägen 14, SE-22362 Lund, Sweden

[e]Department of Chemical Engineering, Technion – Israel Institute of Technology, Haifa 3200003, Israel

[f]Diabetes Service, Department for the Study and Treatment of Abdominal Diseases and Transplants, IRCCS-ISMETT (Istituto Mediterraneo per iTrapianti e Terapie ad Alta Specializzazione), via Tricomi 5, 90127 Palermo, Italy. E-mail: acasu@ismett.edu

[g]Ri.MED Foundation, via Bandiera, 90133 Palermo, Italy
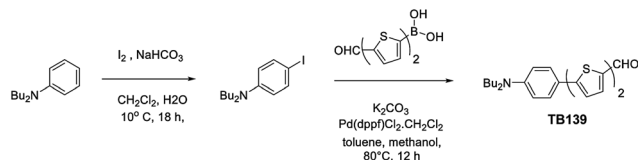
Scheme 1 Synthesis of the fluorescent dye **TB139**.

detection, monitoring of the mechanisms leading to β-cells death, and monitoring of the effect of β-cells replacement therapies (*i.e.*, islet transplantation) are still open, principally because of the difficulty in quantifying the mass of β-cells. To date, no methods are routinely clinically applicable for *in vivo* imaging of these cells. The development and implementation of reliable and accurate technologies for *in vivo* islet imaging is one of the priorities set by scientific committees and societies in the field of diabetes and β-cell transplantation.[16]

A number of strategies for pancreatic β-cell imaging have been attempted in the last 10 years, applying different techniques such as magnetic resonance imaging (MRI), positron emission tomography (PET), single photon emission computed tomography (SPECT), fluorescence, and combinations of them. For the most part, MRI strategies use commercially available iron oxide nanoparticles added to islet preparations before transplantation, with follow-up MRI imaging to detect a signal for up to 6 months after transplantation. There is conflicting data in the literature on long-term imaging capacity, and toxicity to the islets.[17–19] Recently, GLP-1 receptor agonists or antibody-functionalized have been prepared and tested in rats, mice, and non-human primates, with promising results.[20–23] MRI contrast agents for Zn^{2+} sensing have also been tested *in vitro* and *in vivo*.[24,25] Tracers specifically targeted to the β-cells were applied. The most used targets were the GLP-1 receptor and VMAT2 (vesicular monoamine oxidase transporter 2). Specific ligands to these targets were labelled with radioactive compounds for SPECT and PET imaging. These strategies have been tested in animals and in humans to detect insulinomas and transplanted islets.[26–29] Fluorescent dyes have also been applied *in vitro*, *ex vivo* and *in vivo* in animal models quite recently. The most interesting are a fluorescent GLP-1R agonist tested in mice and pigs,[30] and a fluorescent glibenclamide molecule.[31] Even if these approaches are promising and seem to be effective in animal models, the only applications in humans have been in islet transplantation, with limitations in the long-term detection of islets, and in tumour detection. Lack of specificity and high signal-to-noise ratio still limit most of the other strategies.

To assess the potential of cubosomes as an imaging tool for the evaluation of β-cells, we here report the *in vitro* interactions between β-cells and cubosomes loaded with a potent, hydrophobic fluorophore of innovative synthesis (Scheme 1, **TB139**).

2. Experimental section

2.1 Materials and methods

Monoolein (MO, 1-monooleoylglycerol, RYLO MG 19 PHARMA, glycerol monooleate, 98.1 wt%) was kindly provided by Danisco

A/S, DK-7200, Grinsted, Denmark. Pluronic F108 (PEO132-PPO50-PEO132), *N*,*N*-dibutylaniline (97%), NaHCO$_3$ (≥99.7%), K$_2$CO$_3$ (≥99%), Pd(dppf)Cl$_2$, toluene (99.8%), methanol (≥99.8%), dichloromethane (99.8%), and petroleum ether (bp 40–60 °C) were purchased from Sigma-Aldrich. 5′-Formyl-2,2′-bithiophene-5-boronic acid was purchased from TCI. Distilled water passed through a Milli-Q water-purification system (Millipore) was used to prepare the samples.

2.2 Synthesis of the fluorescent probe TB139

N,*N*-Dibutyl-4-iodoaniline obtained by iodination of commercially available *N*,*N*-dibutylanilinein the presence of NaHCO$_3$ (ref. 32) (1.21 g, 3.65 mmol) and 5′-formyl-2,2′-bithiophene-5-boronic acid (0.95 g, 4.01 mmol) were dissolved in toluene (9 mL) and methanol (9 mL) in a dry round bottom flask flushed with argon. K$_2$CO$_3$ (1.25 g, 9.12 mmol) and Pd(dppf)Cl$_2$ (148 mg, 0.18 mmol) were then added under argon, and the reaction mixture stirred at 80 °C for 6 hours. The mixture was filtered through a pad of celite, rinsed with dichloromethane, and the filtrate then concentrated under vacuum. The residue was further purified by silica-gel column chromatography using a 1/1 dichloromethane/petroleum ether mixture to yield 1 g (73%) of the desired compound as an orange solid. M.p. = 110–111 °C. R_f = 0.33 (petroleum ether/dichloromethane (1/1)). ^{1}H NMR (300 MHz, CDCl$_3$) δ 9.83 (s, 1H) 7.65 (d, *J* = 4 Hz, 1H), 7.45 (d, *J* = 8.9 Hz, 2H), 7.29 (d, *J* = 3.8 Hz, 1H), 7.20 (d, *J* = 4 Hz, 1H), 7.07 (d, *J* = 3.9 Hz, 1H), 6.63 (d, *J* = 8.9 Hz, 2H), 3.30 (t, *J* = 7.6 Hz, 4H), 1.59 (quint, *J* = 7.5 Hz, 4H), 1.37 (m, *J* = 7.4 Hz, 4H), 0.96 (t, *J* = 7.3 Hz, 6H). ^{13}C NMR (75 MHz, CDCl$_3$) δ 182.2, 148.1, 148.0, 147.8, 140.6, 137.5, 132.2, 127.3, 126.9, 123.1, 121.3, 120.3, 111.5, 50.7, 29.4, 20.3, 13.9. IR (KBr): 2955, 1661, 1606, 1456, 1231, 1052, 791 cm^{-1}. HRMS (FD) calcd for C$_{23}$H$_{27}$NOS$_2$ (M$^+$) *m/z* 397.15341; found 397.15423. Anal. calcd for C$_{23}$H$_{27}$NOS$_2$: C, 69.48; H, 6.84; N, 3.52. Found: C, 69.35; H, 7.00; N, 3.56.

2.3 Cubosome preparation

Cubosomes were prepared by dispersing the appropriate amount of melted MO in a solution of Pluronic F108 using an ultrasonic processor UP100H by Dr Hielscher, cycle 0.9, amplitude 90%, for 10 minutes. To obtain fluorescent cubosomes, the fluorophore **TB139** was dispersed in the melted monoolein with the help of an ultrasonic bath before dispersion in Pluronic F108. The sample volume was 4 mL with 96.4 wt% of water, 3.3 wt% of MO, and 0.3 wt% of Pluronic F108. The molar concentration of **TB139** was 7.01 × 10^{-4}.

2.4 Dialysis and dye and drug-loading efficiency

TB139 is highly hydrophobic. In order to prove this property, before its encapsulation within cubosomes, solubility tests were carried out. **TB139** was left under stirring in ultrapure water at room temperature overnight, at a nominal concentration equivalent to that present in cubosomes before dialysis (around 8 × 10^{-4} M). Absorbance and fluorescence spectra were acquired on the limpid solution obtained after centrifugation of the sample. A flat line was obtained in both cases, thus proving

the virtually zero solubility in water of the dye. In the light of these experiments we assumed that a dialysis of 2 hours (sample/water of dialysis ratio was equal to 1/500) was largely sufficient for the elimination of the non-encapsulated dye. After loading with **TB139**, the cubosome dispersion was purified from the non-encapsulated dye by dialysis: 2 mL was loaded into a dialysis tubing cellulose membrane (14 kDa MW cutoff) and dialyzed against water (1000 mL) for 2 hours (by replacing the water after 1 hour) at 25 °C. The loading efficiency (E%), expressed as percentage of the amount of the dye present in the formulation before dialysis, was determined by UV-vis spectroscopy after disruption of cubosomes with methanol. **TB139** content was quantified with a Thermo Nicolet Evolution 300 UV-VIS spectrophotometer at 449 nm, and an E% of 87.5 was registered.

2.5 Photophysical characterization

The photophysical properties of fluorescent dye **TB139** were analyzed with freshly prepared air equilibrated solutions at room temperature (20 °C) in spectroscopic grade chloroform. UV/Vis absorption spectra were recorded using a Jasco V-570 spectrophotometer. Steady-state fluorescence measurements were made on dilute solutions (optical density < 0.1) contained in standard 1 cm quartz cuvettes using a Horiba (FluoroLog or FluoroMax) spectrometer in photon-counting mode. Fully corrected emission spectra were obtained at $\lambda_{\text{ex}} = \lambda_{\text{abs}}^{\text{max}}$, with an optical density at $\lambda_{\text{ex}} \leq 0.1$ to minimize internal absorption. Fluorescence quantum yields were measured using cresyl violet in MeOH ($\Phi_{\text{f}} = 0.54$) as a standard. Cubosome dispersions were diluted with Milli-Q water (1 : 300) before making the photophysical measurements. The emission and excitation spectra were recorded with a Perkin Elmer LS 55 spectrofluorimeter.

2.6 Cryogenic transmission electron microscopy (cryo-TEM)

Vitrified specimens were prepared in a controlled environment vitrification system (CEVS) at 25 °C and 100% relative humidity. A drop (~3 μL) of the sample was placed on a perforated carbon film-coated copper grid, blotted with filter paper, and plunged into liquid ethane at its freezing point. The vitrified specimens were transferred to a Gatan 626 cryo-holder and observed at 120 kV acceleration voltage in an FEI Tecnai T12 G^2 transmission electron microscope at about −175 °C in the low-dose imaging mode to minimize electron-beam radiation-damage. Images were digitally recorded with a Gatan US1000 high-resolution CCD camera.

2.7 Small-angle X-ray scattering (SAXS)

The characterization of the nanoparticles' structure as a function of temperature was made with SAXS, using the Ganesha 300XL (SAXSLAB ApS, Skovlunde, Denmark). This instrument is equipped with a 2D 300 K Pilatus detector (Dectris Ltd., Baden, Switzerland) and a Genix 3D X-ray source (Xenocs SA, Sassenage, France), generating X-rays at a wavelength, λ, of 1.54 Å. The scattering data were collected at a q-range of $0.014 < q\ (\text{Å}^{-1}) < 0.753$, where the magnitude of the scattering vector, q, is defined as $q = (4\pi/\lambda)\sin(\theta/2)$, and where θ is the scattering

angle. The two-dimensional scattering pattern was radially averaged using SAXSGui software to obtain $I(q)$. Measurements were made in 1.5 mm quartz capillaries (Hilgenberg GmbH, Malsfeld, Germany). The temperature was controlled by an external, re-circulating water bath within ±0.3 °C. The cubosome formulation was analysed by SAXS without further dilution or treatment. Each scattering measurements was performed for 2 hours after 1 hour of equilibration at the measurement temperature.

Water channels radii of the reverse bi-continuous cubic phases were calculated using the relation $r_{\text{W}} = [(A_0/-2\pi\chi)^{1/2}a] - L$, where L is the length of the lipid hydrophobic chain (17 Å, in case of MO), a is the lattice parameter obtained from the SAXS analysis, and A_0 and χ are the surface area and the Euler characteristic of the infinite periodic minimal surface geometries ($Pn3m$, $A_0 = 1.919$, $\chi = -2$; $Im3m$, $A_0 = 2.345$, $\chi = -4$). At least two Bragg peaks were used to estimate the errors associated with a and r_{W}, unless otherwise indicated.

2.8 Light scattering

Dynamic light scattering (DLS) experiments were done to obtain the size evolution of the nanoparticles as a function of temperature. For this purpose we used a light scattering goniometer instrument (3D LS Spectrometer, LS Instruments, Fribourg, Switzerland), equipped with a 35 mW He–Ne laser light source (wavelength of 632.8 nm). The instrument implements the so-called cross-correlation scheme to suppress contributions from multiple scattering,[33-35] together with a modulation unit.[36] The samples were placed in 10 mm diameter cylindrical borosilicate disposable culture tubes (Fisherbrand, Thermo Fisher Scientific Inc., Waltham, USA), and kept at the measurement temperature in a temperature-controlled index-matching bath. Samples were equilibrated at the measurement temperature for 10 minutes before the experiment. The scattering angle was set at 90°, and each sample was measured at 10, 25, 37, and 50 °C five times for temperature. The initial decay rate, Γ, was derived from the second-order cumulant analysis of the normalized field autocorrelation function, which was used to calculate the apparent collective diffusion coefficient, D_0, of the nanoparticles:

$$\Gamma = D_0 q^2 \tag{1}$$

where q is the module of the scattering vector, $q = (4\pi n/\lambda)\sin(\theta/2)$, with n the refractive index of the solvent, λ the wavelength of the incoming laser light, and θ the scattering angle. The hydrodynamic radius, R_{h}, was obtained with the Stokes–Einstein relation ($D_0 = k_{\text{B}}T/6\pi\eta R_{\text{h}}$), where k_{B} is the Boltzmann constant, T is the absolute temperature, and η is the viscosity of the solvent at the temperature T.

2.9 Cell culture and treatment

The rat pancreatic β-cell line (INS-1E) was cultured in RPMI1640 medium with 11 mM glucose (Invitrogen, USA), supplemented with 10% fetal bovine serum (FBS, Hyclone, USA), 10 mmol L^{-1} HEPES, 1 mM sodium pyruvate, 2 mmol L^{-1} L-glutamine, 50 μM

2-mercaptoethanol, 100 U mL^{-1} penicillin, and 100 μg mL^{-1} streptomycin (Invitrogen, USA) at 37 °C and 5% CO_2.

Cubosomes loaded with **TB139** fluorophore were added to the cell culture at the following concentrations: 5, 10, 20, and 100 μM of cubosomes (in terms of lipid content), at different incubation times, as detailed below.

2.10 Flow cytometric analysis

The internalization efficiency of cubosomes to the cells was investigated with flow cytometry (BD FACS ARIA II instrument, Becton Dickinson Biosciences). INS-1E cells grown at 40–50% confluence were incubated with or without (controls) **TB139**-labeled cubosomes (5–10–20–100 μM in terms of lipid content) for 1, 2, 4, and 24 hours, and analyzed for the evaluation of **TB139** signal. INS-1E cells were detached with 0.05% trypsin–EDTA and washed twice with PBS before flow cytometry analysis. Non-specific fluorescence was evaluated on non-treated cells. The experiment was conducted in triplicate.

2.11 Fluorescence microscopy

The cubosomes' internalization efficiency was also investigated with fluorescence microscopy observation in the same conditions described above. The **TB139** signal was evaluated using EVOS™ fl Digital Inverted Fluorescence Microscope (Fisher Scientific, Paisley, Scotland, UK). Signal intensity was analyzed with ImageJ software (National Institute of health, USA).

2.12 Assay of cell growth (xCELLigence)

Cell growth was measured in real time using xCELLigence technology (ACEA, San Diego, CA). The xCELLigence system was used according to manufacturers' instructions. Briefly, after background impedance determination, INS-1E cells (5 × 10^4 cells per well) were seeded into 16-well E-plates and incubated for 30 minutes at room temperature before installation in the Real-Time CellAnalyzer station in a conventional cell incubator at 37 °C and 5% CO_2. The cells were grown for 48 hours before incubation with or without (control) 5, 10, 20, and 100 μM of cubosomes in the log growth phase. The time point 0 hours was determined when cells were exposed to the nanoparticles. The cells were treated with cubosomes for the duration of entire experiment. The impedance was measured every 15 minutes and expressed as cell index (CI), defined as $(R_n - R_b)/15$, where R_n is the impedance at a given time point, and R_b is the background impedance. Each culture condition was carried out in quadruplicate. The normalized CI was determined by the CI at a given time point divided by the CI at the normalization time point. Slopes of growth curves were determined in the first 24 hours after treatment.

2.13 Cell cycle analysis

The cell cycle was measured by propidium iodide (PI) (Sigma, St. Louis, MO, USA) staining (50 μg mL^{-1}). INS-1E cells 60–70% confluent were incubated with or without (controls) 5, 10, 20, and 100 μM of cubosomes for 24 hours. Cells were then fixed with 1 mL of 70% ethanol in PBS at −20 °C, and then washed once with PBS and subsequently re-suspended in 1 mL PI containing RNAse (250 μg mL^{-1}) for 60 minutes at room temperature, and protected from light. PI fluorescence was detected at an excitation wavelength of 488 nm and an emission wavelength of 575 nm using a BD FACS ARIA II instrument, and was analysed with Diva 6.1.2 software (Becton Dickinson Biosciences). The experiment was conducted in triplicate.

2.14 Apoptosis and necrosis analysis

Apoptosis/necrosis were analyzed with Annexin-V-FITC-PI assay kit following the manufacturer's staining protocols (Annexin-V-Fluos, Roche Applied Sciences, Germany). INS-1E cells 60–70% confluent were incubated with or without (controls) 5, 10, 20, and 100 μM of cubosomes for 24 hours. Annexin-V fluorescence was detected at an excitation wavelength of 488 nm and an emission wavelength of 525 nm, while PI fluorescence was detected at an excitation wavelength of 488 nm and an emission wavelength of 575 nm using a BD FACS ARIA II instrument. The experiment was conducted in triplicate and the data were analyzed with Diva 6.1.2 (Becton Dickinson Biosciences).

2.15 Statistics

At least three independent experiments were done for each condition, and were expressed as the mean ± standard deviation (SD). Data from different groups were compared using the Student's t test. Differences between the groups were considered significant at a value of $p < 0.05$.

3. Results and discussion

3.1 Physicochemical and photophysical characterization of fluorescent cubosomes

The lipophilic fluorescent probe **TB139** was prepared *via* a multistep synthesis from the commercially available *N,N*-dibutylaniline (Scheme 1). First *N,N*-dibutyl-4-iodoaniline was obtained by iodination of *N,N*-dibutylanilinein the presence of $NaHCO_3$, then subjected to a Suzuki–Miyaura cross-coupling with 5′-formyl-2,2′-bithiophen-5-boronic acid leading to **TB139** in 73% yield. This dye is highly soluble in organic environments. It strongly absorbs in the UV and visible region, and emits in the visible region. The intense low-energy absorption band ($\lambda_{abs}^{max} = 451$ nm, $\varepsilon^{max} = 3.1 \times 10^4$ M^{-1}) is characteristic of an intramolecular charge transfer (ICT) transition. The dye is also a bright yellow-orange emitter in low to medium polarity solvents ($\lambda_{em}^{max} = 608$ nm, $\Phi_f = 0.84$ in $CHCl_3$). Moreover, **TB139** offers the advantage of a high quantum yield also after encapsulation inside the cubosomes ($\Phi = 0.39$).

A cryo-TEM[37] image of the fluorescent cubosomes formulation is shown in Fig. 1. A number of quasi-spherical nanoparticles are discernible showing a dense, dark inner nanostructure (the lipid bilayers) intersected by a regular alternation of bright spots (the water channels). As often occurs in cubosome formulations, the presence of small unilamellar vesicles is also noticed.

To definitively assess the nanostructure of these nanoparticles, the formulation was further investigated with SAXS
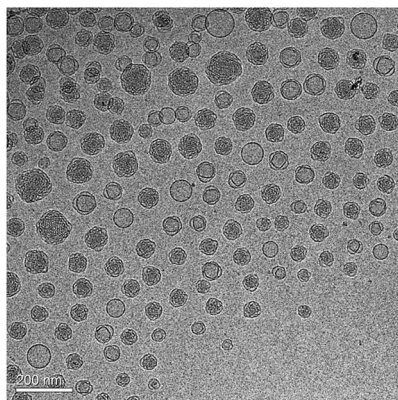
Fig. 1 Cryo-TEM image of the cubosome formulation loaded with the **TB139** fluorescent probe.

Table 1 Cubosome lattice parameters (a)

T (°C)	Pn3m		Im3m[a]	
	a (Å)	r_W (Å)	a (Å)	r_W (Å)
25	98 ± 1	21 ± 1	124	21
37	90 ± 1	18 ± 1	116	18

[a] Standard deviations on a and r_W are not reported because these parameters were obtained from a single Bragg peak.

and DLS. Moreover, these physicochemical characterizations were made at both room and physiological temperature. Diffractograms acquired on cubosomes loaded with **TB139** at 25 and 37 °C are shown in Fig. 2. At least four Bragg peaks were detected with relative positions $\sqrt{2}:\sqrt{3}:2:\sqrt{6}$, indexed as the (110), (111), (200), and (211) reflections of a double diamond inverse bicontinuous cubic phase (*Pn3m* crystallographic space group). However, a weak reflection at low q, indexed as the (110) reflection of a primitive inverse bicontinuous cubic phase (*Im3m* crystallographic space group), revealed that the cubosomes' nanostructure is, indeed, biphasic. The coexistence of the two bicontinuous cubic phases is well documented in literature, and can be ascribed to the *Pn3m* to *Im3m* intercubic phase transition provoked by the Pluronic used to stabilize the formulation against coalescence when, after saturation of the surface of the cubosomes, this polymer starts to be incorporated with the monoolein, participating to the formation of the inner structure of the nanoparticles.[38,39]

The lattice parameters, a, and the water channels radii, r_W, calculated for both these bicontinuous cubic phases are reported in Table 1, and indicates that the nanostructure is basically not altered by the increase in temperature, though the structure slightly shrinks (a and r_W decrease) because of the

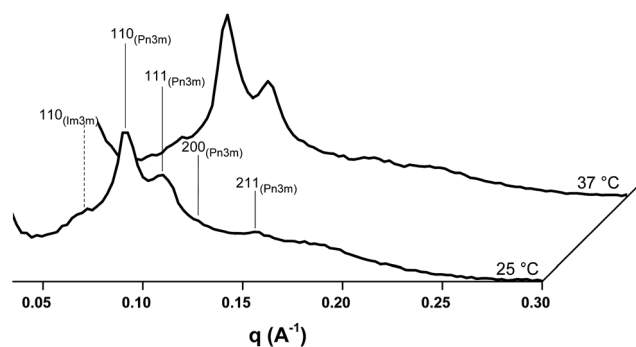higher negative curvature at the lipid/water interface induced by the enhanced disorder of the MO chains at higher temperature.

DLS results confirmed that the size and the polydispersity of the nanoparticles are also unaffected by the temperature increase, with the formulation showing an average hydrodynamic radius of 80 nm, and a polydispersity index of 0.15 at both tested temperatures. These results are fully comparable to others previously reported by our group concerning empty cubosome formulations (not loaded with drugs and/or imaging probes).[40,41] This fact confirms that the insertion of the **TB139** fluorescent probe within the lipid matrix (at the concentration here used) neither altered the local MO dynamics nor its effective packing parameter,[42] with the preservation of the original nanostructure.

The emission and excitation spectra of the cubosome formulations recorded after 1 : 300 dilution in ultrapure water are reported in Fig. 3. Excitation at 449 nm results in an emission at 600 nm (solid line), and the excitation spectra fixed at 600 nm (dashed line) is in perfect accordance with the absorption spectrum of the free dye in CHCl₃ (see inset in Fig. 3 solid line). Due to the turbidity of the dispersion, the determination of the quantum yield of the dye in the nanoparticles was not feasible.

3.2 Cell internalization

To evaluate the potential of this cubosome formulation as a diagnostic tool in diabetes, it is essential to examine their uptake in β-cells. For this purpose, a rat pancreatic β-cell line (INS-1E) was incubated without (controls) or with different concentrations of cubosomes. Different exposure times were

Fig. 2 I(q) vs. q data obtained by SAXS experiments performed on the same cubosome formulation as in Fig. 1 at 25 and 37 °C. The Miller indices are reported above the corresponding Bragg peaks, with the indication of the space group.
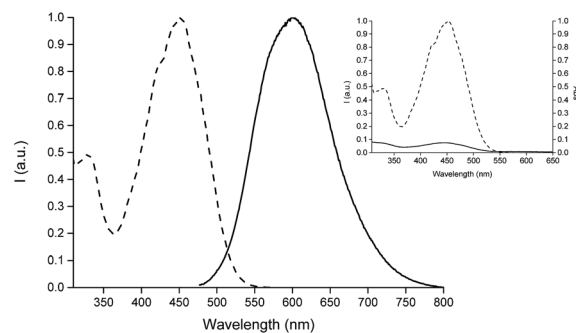

Fig. 3 Normalized emission (dashed line, λ_{exc} = 449 nm) and excitation (solid line, λ_{em} = 600 nm) spectra of the aqueous cubosome formulation.

chosen (1, 2, 4, and 24 hours) with the aim of mimicking exposure after a bolus administration or continuous infusion or re-circulation. The internalization efficiency was evaluated in parallel with imaging under microscope and flow cytometry quantification. After incubation, cubosome red fluorescence was distributed homogeneously inside the cells but outside of the nucleus.

Fig. 4A shows some representative images of INS-1E cells after cubosome internalization. A progressive increase of the fluorescent signal was detected with time and concentration, and this was confirmed by both fluorescence intensity analysis (Fig. 4B) and flow-cytometric analysis (Fig. 4C) of the INS-1E cells incubated with cubosomes. With both methods, the fluorescence was detectable at all times, only after exposure of cells to 100 μM cubosome solution. At lower concentrations, the fluorescence was detectable after 2 hours exposure, increased after 4 hours and reached a plateau at 24 hours exposure.

At 5 μM concentration fluorescence was detectable only after 4 and 24 hours incubation. Flow-cytometric analyses showed the signal persistence up to 24 hours, and a reduction of mean fluorescence intensity after 72 hours, likely caused by the split

of fluorescence into separate cell populations due to the cell duplication process (data not shown).

3.3 Assessment of cell cytotoxicity

The potential cytotoxicity of monoolein-based cubosomes against various cell lines was recently explored in different papers by several authors, showing a certain degree of cellular toxicity induced by monoolein-based cubosomes. Such cytotoxicity varies depending on the formulation (monoolein/Pluronic ratio, type of Pluronic used) and, particularly, by the cell line investigated.[40,43–47] Remarkably, haemolytic properties of this kind of nanoparticles were also reported,[48] although the formulation can be adapted to minimize/avoid this drawback.[49] Here, the toxic effect of the cubosomes formulation containing the **TB139** fluorophore was assessed in a pancreatic β-cell line. The effect on cell growth after exposure to 5, 10, 20 or 100 μM of cubosome formulation was evaluated by means of a real time analysis of proliferation carried out with an xCELLigence
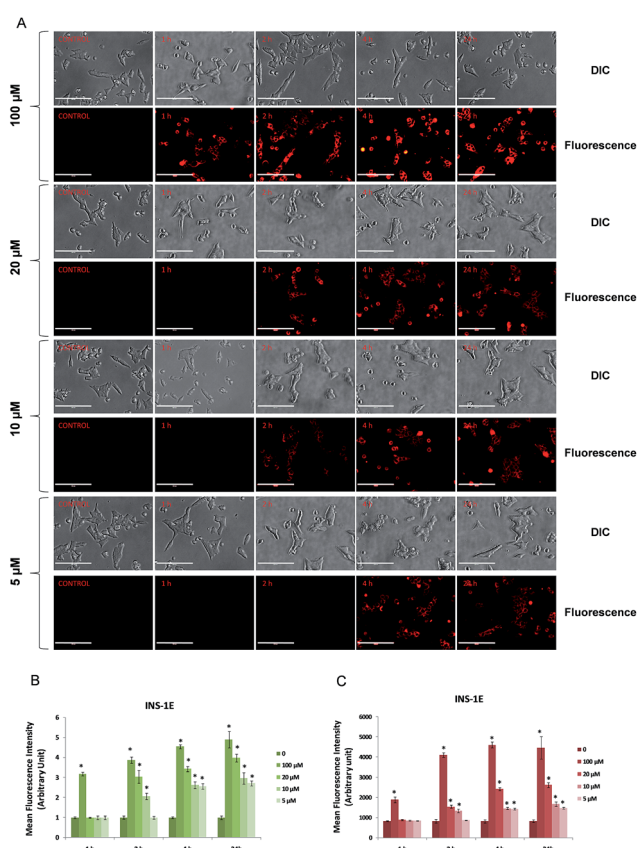
Fig. 4 Microscopy and FACS analysis of NPs internalization. INS-1E cells were incubated with or without (control) 5−10−20−100 μM NPs for 1−2−4−24 hours. (A) Representative images at different time points and concentrations are shown. Scale bar corresponds to 100 μm. (B) Red fluorescence intensity analyzed by ImageJ software. (C) Flow-cytometric analyses of NPs internalization. DIC: differential interference contrast. All data are expressed as means ± SD of triplicates. *p < 0.05 versus control.
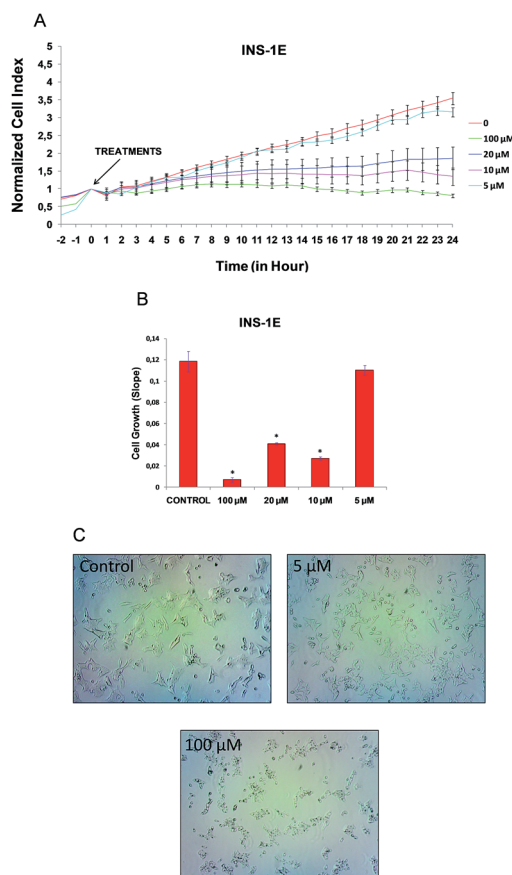
Fig. 5 INS-1E cells growth. INS-1E cells were incubated with or without (control) 5−10−20−100 μM NPs to test their cytotoxicity. (A) Real-time growth monitoring of INS-1E using the xCELLigence system. Cell index values were recorded by the xCELLigence system every 15 min and representative traces +95% CI are shown. (B) Slopes of growth curves. (C) Representative cell morphology examined using phase-contrast microscopy with and without NPs at lowest concentration (5 μM) and higher concentration (100 μM) after 24 h cultures (magnification, ×4). Data are means ± SD of n = 4. *p < 0.05 versus control.

system. Cell proliferation capacity was considered an indicator of cell wellbeing. Only the proliferation curves relative to the 5 μM NPs were comparable to the untreated cultures. In contrast, when compared with the control, significant reduction in the cell index (CI) values was observed for INS-1E cells treated with 10–20–100 μM cubosome formulation (Fig. 5A and B). Moreover, INS-1E cells underwent severe loss of morphology when exposed to 100 μM of cubosomes for 24 hours, while there was no change in morphology when treated with 5 μM of cubosomes. This indicates that cells exposed to the cubosomes at 5 μM concentration preserved their viability, spreading capacity, and structure over the observation period (Fig. 5C).

Because an effect was seen on cell proliferation, a more in-depth analysis was done to identify which step of the cell cycle entry and progression was affected. As shown in Fig. 6A the number of cells blocked in the G2–M phase increased (5.9%, 6.2%, 5%) after 24 hours of 100, 20, and 10 μM cubosome treatment, respectively, compared with untreated cells (3.9%), while the 5 μM cubosome formulation did not show any effect on the number of blocked cells in G2–M (4.2%) as compared with untreated cells. No significant difference of cell populations in G0–G1 and S phase after 24 hours of treatment was seen at any of the concentrations applied (Fig. 6A). A significant reduction of apoptotic cellsupon exposure to the cubosome formulation at 5 μM (2.15%) compared to exposure to 100, 20, and 10 μM cubosome formulation (8.4%, 5.2% and 5.6% respectively) was seen. A more in depth analysis of apoptosis was then done with Annexin V/propidium iodide staining. Only 5 μM cubosome treatment did not significantly affect apoptosis/necrosis (2% and 3.85% respectively) if compared to control (1.85% and 2.95% respectively), while a significant apoptosis was induced by 100, 20, 10 μM cubosome treatment. Also a significant necrosis was induced by 100, 20, 10 μM cubosome treatment (20.7%, 7.9% and 5.4% respectively). Therefore, the cell cycle and apoptosis/necrosis analysis confirmed what was seen through the xCELLigence apparatus, with minimal or no effect of 5 μM concentration on cell wellbeing. The reduction of cell proliferation with higher cubosome concentrations seems related to an increased cell apoptosis/necrosis and block in the G2–M phase.

4. Conclusions

Fluorescent cubosome nanoparticles were formulated by embedding within the monoolein palisade a newly synthesized dye, **TB139**. The physicochemical analysis, conducted by cryo-TEM, SAXS, and DLS confirmed that **TB139** can be incorporated in the nanoparticles without altering the original morphological and topological features of the monoolein-based cubosomes. The photophysical investigation demonstrated that encapsulation of **TB139** within the cubosomes did not alter the fluorescent properties of the dye. Compared to other dyes suitable for biomedical applications that emit in the same spectral window (around 600 nm), **TB139** offers the advantage of a high quantum yield both in organic solvents and inside the cubosomes. The cubosome formulation was then tested at different concentrations for the imaging of a β-cell line, showing that it is internalized by the cells, and is well tolerated when used at low concentrations. This result was achieved thanks to the powerful fluorescent dye chosen, which allowed the reduction of cubosome concentration to be applied to the cells, maintaining clear fluorescence detection with either microscope imaging or flow cytometry.

Recently, various examples of commercially available or synthetically modified fluorescent dyes were proposed for the imaging of β-cells, both *in vitro* and *in vivo* (VT750, AF680, bodipy analogous, rhodamine derivatives, just to cite a few).[30,31,50–54] The concentrations used were normally in the range 1–50 μM. However, in some cases the concentration of the dyes could be as low as nanomolar level, as in our case. Indeed, **TB139** is 3.77×10^{-8} M in the 5 μM monoolein sample, although it allows the imaging of the β-cells still after 24 hours. Remarkably, although some examples of magnetic nanoparticles for MRI imaging have been reported in the literature,[55,56] to the best of our knowledge, the formulation here proposed is the first example of nanoparticles developed so far for the fluorescent imaging of β-cells.[57]
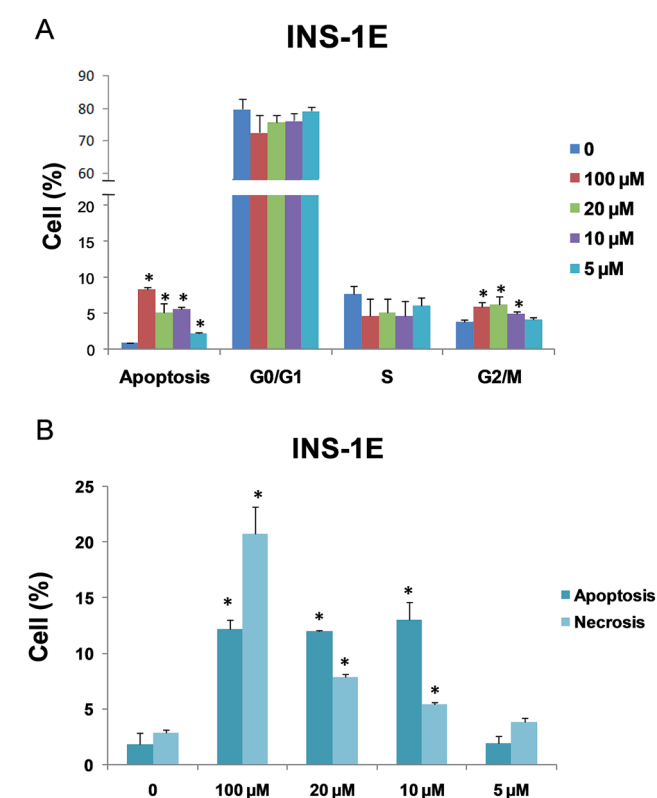

Fig. 6 Cycle arrest and apoptosis in INS-1E cells. INS-1E cells were incubated with or without (control) 5–10–20–100 μM NPs for 24 h. (A) DNA content of cells was visualized by propidium iodide staining and analyzed by flow cytometry. DNA content was divided by phases: apoptosis (sub-G1 phase), G0/G1 phase, S phase and G2/M phase. (B) Apoptosis and necrosis levels were determined by Annexin-V/PI assay. Values represent the percentage of cells undergoing each form of death. All data are expressed as means ± SD of triplicates. *$p < 0.05$ *versus* control.

Given their similarity to liposomes, cubosomes have always attracted great attention as possible nanocarriers for IV administration. However, papers devoted to this topic have mainly focused on the use of cubosomes in cancer treatments, although other uses of this kind of nanoparticles, *e.g.* for siRNA delivery, were reported.[58,59] Here, we successfully evaluated the use of these cubic liquid crystalline nanoparticles as tools for the imaging of pancreatic β-cells, revealing their potential for future *in vitro* and *in vivo* applications in diabetes diagnosis and treatments.

Acknowledgements

References

1 T. Lammers, S. Aime, W. E. Hennink, G. Storm and F. Kiessling, *Acc. Chem. Res.*, 2011, **44**, 1029–1038.

2 O. Veiseh, J. W. Gunn and M. Zhang, *Adv. Drug Delivery Rev.*, 2010, **62**, 284–304.

3 J. A. Barreto, W. O'Malley, M. Kubeil, B. Graham, H. Stephan and L. Spiccia, *Adv. Mater.*, 2011, **23**, H18–H40.

4 A. Z. Wang, R. Langer and O. C. Farokhzad, *Annu. Rev. Med.*, 2012, **63**, 185198.

5 I. D. Azmi, S. M. Moghimi and A. Yaghmur, *Ther. Delivery*, 2015, **6**, 1347–1364.

6 X. Mulet, B. J. Boyd and C. J. Drummond, *J. Colloid Interface Sci.*, 2013, **393**, 1–20.

7 M. Monduzzi, S. Lampis, S. Murgia and A. Salis, *Adv. Colloid Interface Sci.*, 2014, **205**, 48–67.

8 S. T. Hyde, *Curr. Opin. Solid State Mater. Sci.*, 1996, **1**, 653–662.

9 S. Hyde, B. W. Ninham, S. Andersson, K. Larsson, T. Landh, Z. Blum and S. Lidin, *The Language of Shape*, Elsevier, 1997.

10 K. Larsson, *Nature*, 1983, **304**, 664.

11 T. Landh, *J. Phys. Chem.*, 1994, **98**, 8453–8467.

12 V. Meli, C. Caltagirone, A. M. Falchi, S. T. Hyde, V. Lippolis, M. Monduzzi, M. Obiols-Rabasa, A. Rosa, J. Schmidt, Y. Talmon and S. Murgia, *Langmuir*, 2015, **31**, 9566–9575.

13 J. Zhai, J. A. Scoble, N. Li, G. Lovrecz, L. J. Waddington, N. Tran, B. W. Muir, G. Coia, N. Kirby, C. J. Drummond and X. Mulet, *Nanoscale*, 2015, **7**, 2905–2913.

14 C. Caltagirone, A. M. Falchi, S. Lampis, V. Lippolis, V. Meli, M. Monduzzi, L. Prodi, J. Schmidt, M. Sgarzi, Y. Talmon, R. Bizzarri and S. Murgia, *Langmuir*, 2014, **30**, 6228–6236.

15 S. Aleandri, D. Bandera, R. Mezzenga and E. M. Landau, *Langmuir*, 2015, **31**, 12770–12776.

16 S. T. Bartlett, J. F. Markmann, P. Johnson, O. Korsgren, B. J. Hering, D. Scharp, T. W. H. Kay, J. Bromberg, J. S. Odorico, G. C. Weir, N. Bridges, R. Kandaswamy, P. Stock, P. Friend, M. Gotoh, D. K. C. Cooper, C.-G. Park, P. O'Connell, C. Stabler, S. Matsumoto, B. Ludwig, P. Choudhary, B. Kovatchev, M. R. Rickels, M. Sykes, K. Wood, K. Kraemer, A. Hwa, E. Stanley, C. Ricordi, M. Zimmerman, J. Greenstein, E. Montanya and T. Otonkoski, *Report from IPITA-TTS Opinion Leaders Meeting on the Future of β-Cell Replacement*, 2016, vol. 100.

17 S. Borot, L. A. Crowe, G. Parnaud, F. Ris, R. Meier, L. Giovannoni, Y. D. Müller, S. Lacotte, P. Morel, C. Toso, D. Bosco, J.-P. Vallee and T. Berney, *Transplantation*, 2013, **96**, 438–444.

18 M. L. Malosio, A. Esposito, A. Poletti, S. Chiaretti, L. Piemonti, R. Melzi, R. Nano, F. Tedoldi, T. Canu, P. Santambrogio, C. Brigatti, F. De Cobelli, P. Maffi, A. Secchi and A. Del Maschio, *Am. J. Transplant.*, 2009, **9**, 2372–2382.

19 M. L. Malosio, A. Esposito, C. Brigatti, A. Palmisano, L. Piemonti, R. Nano, P. Maffi, F. De Cobelli, A. Del Maschio and A. Secchi, *Cell Transplant.*, 2015, **24**, 2285–2296.

20 D. Z. Balla, S. Gottschalk, G. Shajan, S. Ueberberg, S. Schneider, M. Hardtke-Wolenski, E. Jaeckel, V. Hoerr, C. Faber, K. Scheffler, R. Pohmann and J. Engelmann, *Contrast Media Mol. Imaging*, 2013, **8**, 495–504.

21 P. Wang, C. Schuetz, P. Vallabhajosyula, Z. Medarova, A. Tena, L. Wei, K. Yamada, S. Deng, J. F. Markmann, D. H. Sachs and A. Moore, *Transplantation*, 2015, **99**, 1574–1581.

22 L. Vinet, S. Lamprianou, A. Babič, N. Lange, F. Thorel, P. L. Herrera, X. Montet and P. Meda, *Diabetologia*, 2015, **58**, 304–312.

23 B. Yang, H. Cai, W. Qin, B. Zhang, C. Zhai, B. Jiang and Y. Wu, *Int. J. Nanomed.*, 2013, **8**, 3977–3990.

24 A. J. M. Lubag, L. M. De Leon-rodriguez, S. C. Burgess and A. D. Sherry, *PNAS*, 2011, **108**, 18400–18405.

25 G. J. Stasiuk, F. Minuzzi, M. Sae-Heng, C. Rivas, H. P. Juretschke, L. Piemonti, P. R. Allegrini, D. Laurent, A. R. Duckworth, A. Beeby, G. A. Rutter and N. J. Long, *Chem.–Eur. J.*, 2015, **21**, 5023–5033.

26 E. Christ, D. Wild, S. Ederer, M. Béhé, G. Nicolas, M. E. Caplin, M. Brändle, T. Clerici, S. Fischli, C. Stettler, P. J. Ell, J. Seufert, B. Gloor, A. Perren, J. C. Reubi and F. Forrer, *Lancet Diabetes Endocrinol.*, 2013, **1**, 115–122.

27 M. Brom, L. Joosten, C. Frielink, O. Boerman and M. Gotthardt, *Diabetes*, 2015, **64**, 1324–1328.

28 A. Garcia, A. Venugopal, M.-L. Pan and J. Mukherjee, *Diabetes Technol. Ther.*, 2014, **16**, 640–643.

29 F. Pattou, J. Kerr-Conte and D. Wild, *N. Engl. J. Med.*, 2010, **363**, 1289–1290.

30 T. Reiner, G. Thurber, J. Gaglia, C. Vinegoni, C. W. Liew, R. Upadhyay, R. H. Kohler, L. Li, R. N. Kulkarni, C. Benoist, D. Mathis and R. Weissleder, *Proc. Natl. Acad. Sci. U. S. A.*, 2011, **108**, 12815–12820.

31 A. Babič, S. Lamprianou, L. Vinet, N. Stransky-Heilkron, C. Xayaphoummine, M. A. Campo, H. Glombik, A. Schulte, H. P. Juretschke, X. Montet, P. Meda and N. Lange, *Biomaterials*, 2016, **75**, 1–12.

32 O. Mongin, T. R. Krishna, M. H. V. Werts, A.-M. Caminade, J.-P. Majoral and M. Blanchard-Desce, *Chem. Commun.*, 2006, 915–917.

33 G. D. J. Phillies, *Phys. Rev. A At., Mol., Opt. Phys.*, 1981, **24**, 1939–1943.

34 K. Schätzel, *J. Mod. Opt.*, 1991, **38**, 1849–1865.

35 C. Urban and P. Schurtenberger, *J. Colloid Interface Sci.*, 1998, **207**, 150–158.

36 I. D. Block and F. Scheffold, *Rev. Sci. Instrum.*, 2010, **81**, 123107.

37 Y. Talmon, *J. Mol. Liq.*, 2015, **210**, 2–8.

38 M. Nakano, A. Sugita, H. Matsuoka and T. Handa, *Langmuir*, 2001, **17**, 3917–3922.

39 J. Gustafsson, H. Ljusberg-Wahren, M. Almgren and K. Larsson, *Langmuir*, 1997, **13**, 6964–6971.

40 S. Murgia, A. M. Falchi, V. Meli, K. Schillén, V. Lippolis, M. Monduzzi, A. Rosa, J. Schmidt, Y. Talmon, R. Bizzarri and C. Caltagirone, *Colloids Surf., B*, 2015, **129**, 87–94.

41 A. M. Falchi, A. Rosa, A. Atzeri, A. Incani, S. Lampis, V. Meli, C. Caltagirone and S. Murgia, *Toxicol. Res.*, 2015, **4**, 1025–1036.

42 S. Murgia, F. Caboi and M. Monduzzi, *Chem. Phys. Lipids*, 2001, **110**, 11–17.

43 B. W. Muir, D. P. Acharya, D. F. Kennedy, X. Mulet, R. A. Evans, S. M. Pereira, K. L. Wark, B. J. Boyd, T.-H. Nguyen, T. M. Hinton, L. J. Waddington, N. Kirby, D. K. Wright, H. X. Wang, G. F. Egan and B. A. Moffat, *Biomaterials*, 2012, **33**, 2723–2733.

44 S. Murgia, A. M. Falchi, M. Mano, S. Lampis, R. Angius, A. M. Carnerup, J. Schmidt, G. Diaz, M. Giacca, Y. Talmon and M. Monduzzi, *J. Phys. Chem. B*, 2010, **114**, 3518–3525.

45 S. Deshpande, E. Venugopal, S. Ramagiri, J. R. Bellare, G. Kumaraswamy and N. Singh, *ACS Appl. Mater. Interfaces*, 2014, **6**, 17126–17133.

46 T. M. Hinton, F. Grusche, D. Acharya, R. Shukla, V. Bansal, L. J. Waddington, P. Monaghan and B. W. Muir, *Toxicol. Res.*, 2014, **3**, 11–22.

47 N. Tran, X. Mulet, A. M. Hawley, T. M. Hinton, S. T. Mudie, B. W. Muir, E. C. Giakoumatos, L. J. Waddington, N. M. Kirby and C. J. Drummond, *RSC Adv.*, 2015, **5**, 26785–26795.

48 J. Barauskas, C. Cervin, M. Jankunec, M. Špandyreva, K. Ribokaitė, F. Tiberg and M. Johnsson, *Int. J. Pharm.*, 2010, **391**, 284–291.

49 V. Jain, N. K. Swarnakar, P. R. Mishra, A. Verma, A. Kaul, A. K. Mishra and N. K. Jain, *Biomaterials*, 2012, **33**, 7206–7220.

50 N. Y. Kang, S. C. Lee, S. J. Park, H. H. Ha, S. W. Yun, E. Kostromina, N. Gustavsson, Y. Ali, Y. Chandran, H. S. Chun, M. Bae, J. H. Ahn, W. Han, G. K. Radda and Y. T. Chang, *Angew. Chem., Int. Ed.*, 2013, **52**, 8557–8560.

51 S. M. Clardy, E. J. Keliher, J. F. Mohan, M. Sebas, C. Benoist, D. Mathis and R. Weissleder, *Bioconjugate Chem.*, 2014, **25**, 171–177.

52 J. Broichhagen, M. Schönberger, S. C. Cork, J. A. Frank, P. Marchetti, M. Bugliani, A. M. J. Shapiro, S. Trapp, G. A. Rutter, D. J. Hodson and D. Trauner, *Nat. Commun.*, 2014, **5**, 5116.

53 B. K. Agrawalla, Y. Chandran, W. H. Phue, S. C. Lee, Y. M. Jeong, S. Y. D. Wan, N. Y. Kang and Y. T. Chang, *J. Am. Chem. Soc.*, 2015, **137**, 5355–5362.

54 L. Zhang, T. Navaratna, J. Liao and G. M. Thurber, *Bioconjugate Chem.*, 2015, **26**, 329–337.

55 P. Wang, B. Yoo, J. Yang, X. Zhang, A. Ross, P. Pantazopoulos, G. Dai and A. Moore, *Diabetes*, 2014, **63**, 1465–1474.

56 K. Oishi, Y. Miyamoto, H. Saito, K. Murase, K. Ono, M. Sawada, M. Watanabe, Y. Noguchi, T. Fujiwara, S. Hayashi and H. Noguchi, *PLoS One*, 2013, **8**, 4–10.

57 M. J. Kim and D. Y. Lee, *Macromol. Res.*, 2016, **24**, 197–204.

58 H. Kim and C. Leal, *ACS Nano*, 2015, **9**, 10214–10226.

59 G. Zhen, T. M. Hinton, B. W. Muir, S. Shi, M. Tizard, K. M. McLean, P. G. Hartley and P. Gunatillake, *Mol. Pharm.*, 2012, **9**, 2450–2457.